iScience, Volume *25*

Supplemental information

Remodeling the conformational dynamics of I-motif DNA by helicases in ATP-independent mode at acidic environment

Bo Gao, Ya-Ting Zheng, Ai-Min Su, Bo Sun, Xu-Guang Xi, and Xi-Miao Hou

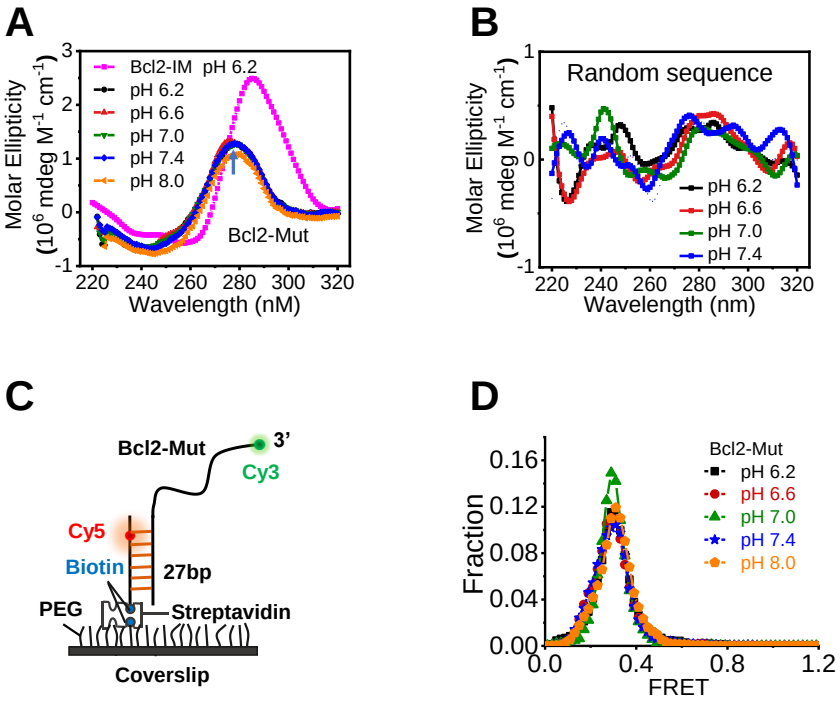

Figure S1. The Bcl2-Mut and the random single-stranded DNA sequences both display little changes with the increases in pH values. Related to Figure 1. (A-B) CD spectrum of Bcl2-Mut and the 20-nt random ssDNA at different pH. This random sequence does not have a distinctive peak or valley. However, Bcl2-Mut displays a characteristic peak at 275 nm indicated by the arrow, which is different from the typical peak of Bcl2-IM at 285 nm as well as the spectrum of random sequence, probably reflecting the formation of some unknown secondary structures as C^+:C base pairs may be formed in this sequence. **(C)** The schematic design of smFRET experiment. The 3'-partial duplex DNA with Bcl2-Mut sequence was anchored onto the coverslip via the 27-bp stem. **(D)** FRET distributions of Bcl2-Mut at different pH.

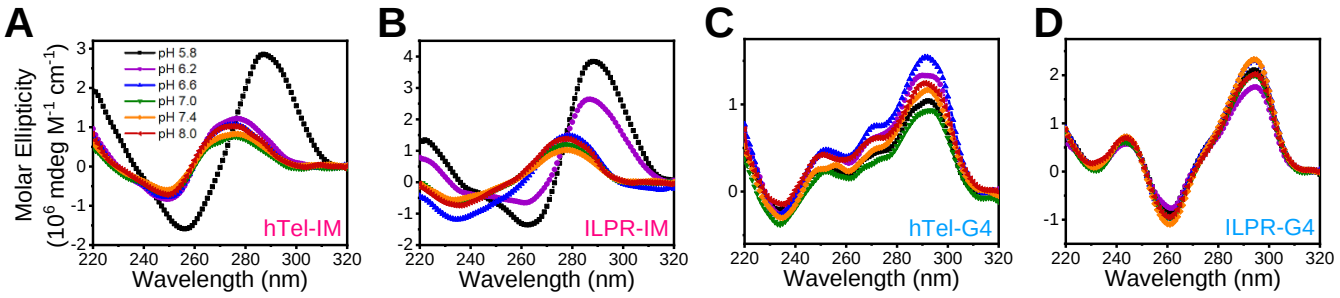

Figure S2. CD spectrum of different i-motif and G4 DNA. Related to Figure 1. (A-B) CD spectrum of i-motif DNA formed at different pH with the sequences from human telomere, and ILPR promoter. **(C-D)** CD spectrum of G4 DNA formed at different pH with the sequences from human telomere, and ILPR promoter.

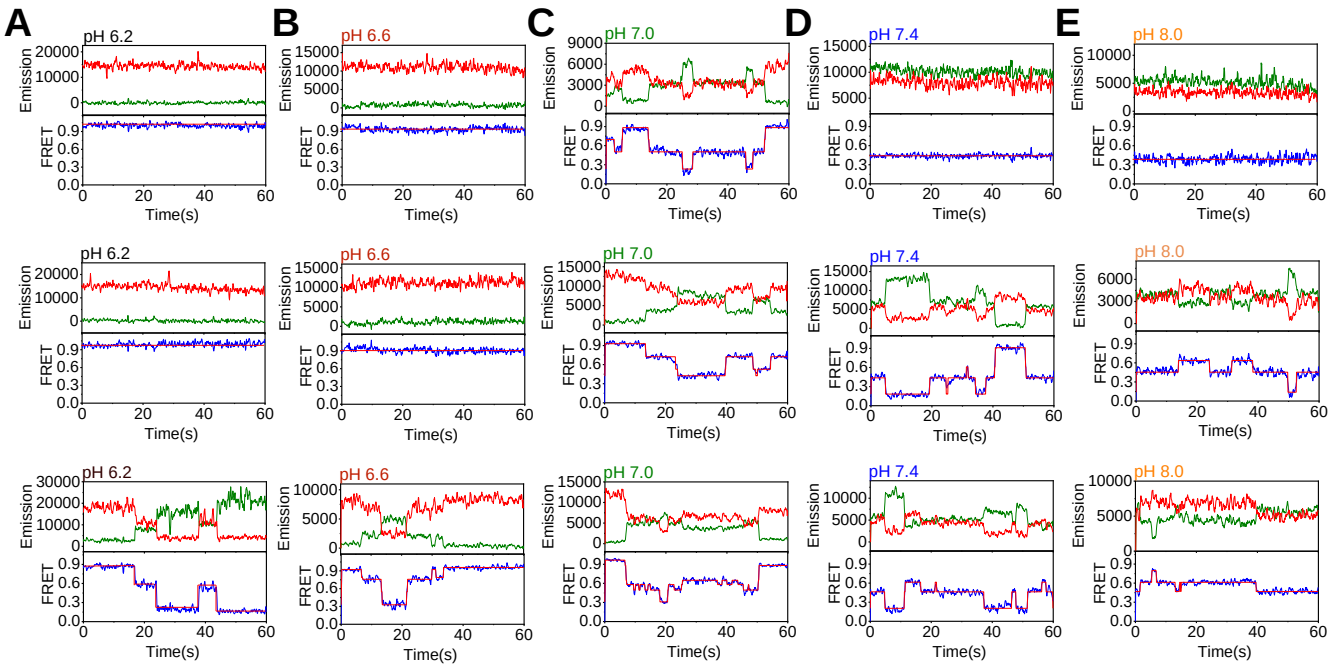

Figure S3. The representative fluorescence and FRET traces of Bcl2-IM at different pH. Related to Figure 2. (A-B) At pH 6.2 and pH 6.6, the majority of traces are static at ~$E_{0.95}$. **(C)** At pH 7.0, the majority of traces are dynamic with slow transitions between different states. **(D-E)** At pH 7.4 and pH 8.0, the majority of traces are dynamic. For the static traces, FRET values are maintained at ~$E_{0.45}$.

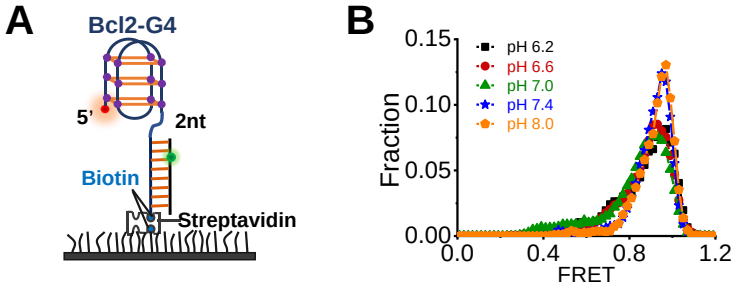

Figure S4. G4s display little changes with the increases in pH. Related to Figure 2. (A) The schematic design of smFRET experiment for Bcl2-G4. G4 DNA was placed at the 5'-end of the duplex. **(B)** FRET distributions of Bcl2-G4 at different pH.

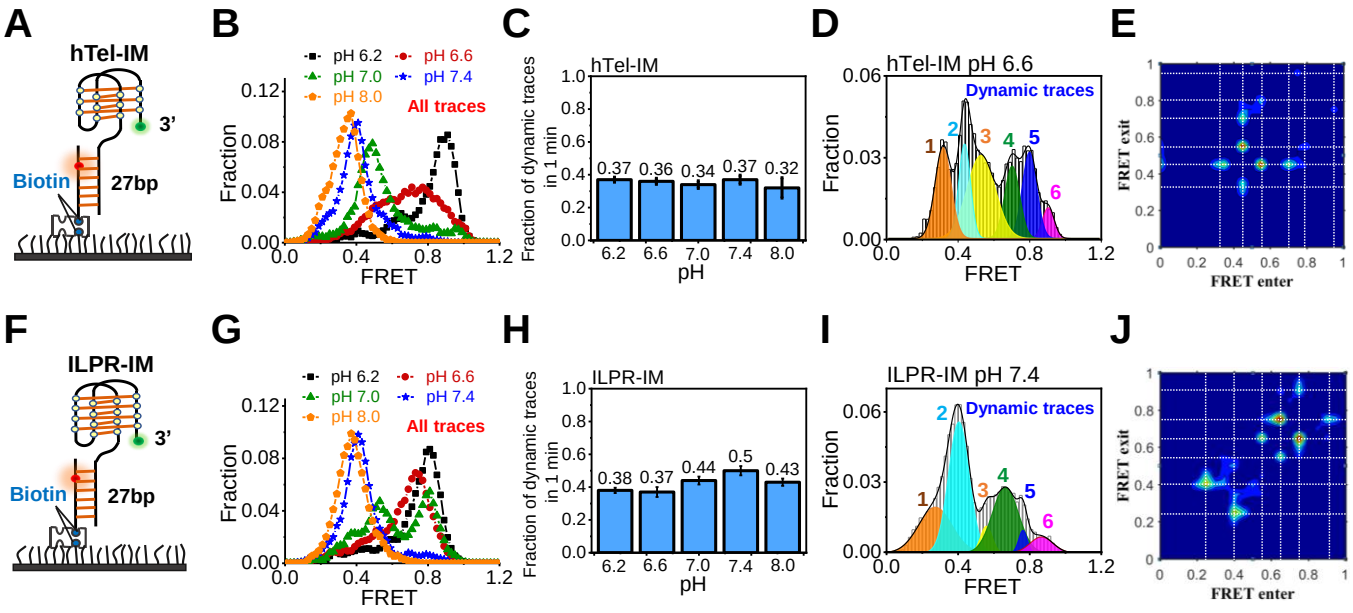

Figure S5. The i-motifs from the human telomere and ILPR promoter display six folding states. Related to Figure 2. (A) The schematic design of smFRET experiment for hTel-IM. **(B)** FRET distributions of hTel-IM at different pH. All traces were included whether it was static or dynamic. **(C)** The fractions of FRET traces showing dynamic changes during the 1-min recording time. Data are represented as mean ± SEM**. (D)** FRET distribution of the dynamic hTel-IM traces at pH 6.6. **(E)** The transition density plot (TDP) of the dynamic hTel-IM traces at pH 6.6. The dashed lines indicate the six different FRET states. **(F)** The schematic design of smFRET experiment for ILPR-IM. **(G)** FRET distributions of ILPR-IM at different pH. All traces were included whether it was static or dynamic. **(H)** The fractions of FRET traces showing dynamic changes during the 1-min recording time. Data are represented as mean ± SEM**. (I)** FRET distribution of the dynamic ILPR-IM traces at pH 7.4. **(J)** The transition density plot (TDP) of the dynamic ILPR-IM traces at pH 7.4. The dashed lines indicate the six different FRET states.

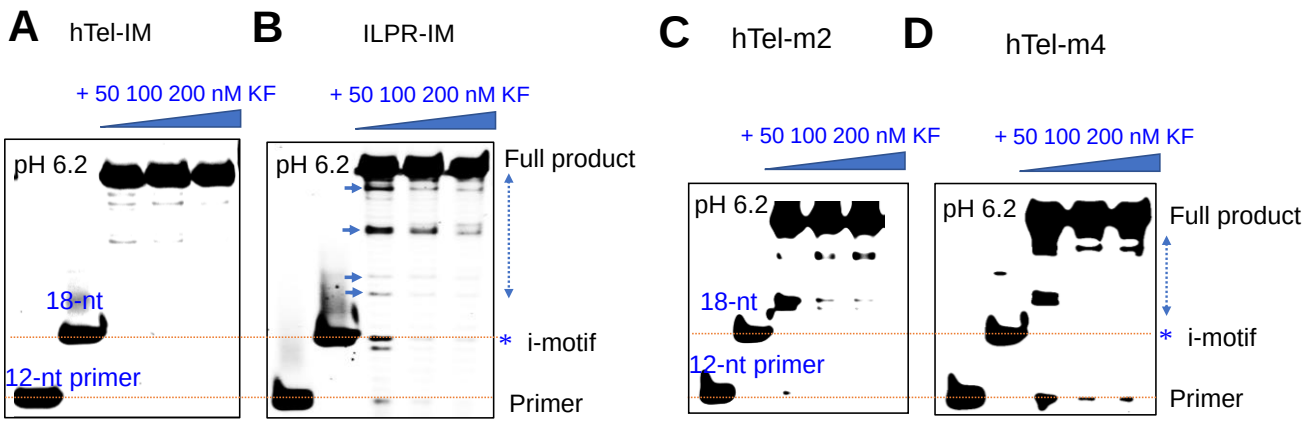

Figure S6. KF stop assay with different i-motif templates at pH 6.2. Related to Figure 2. DNA template was 1 μM and 50-200 nM KF was used. The bottom line shows the position of the 12-nt primer. The other line indicates the 18-nt FAM labelled sequence which mimics the polymerization of 6-nt poly-T linker only (Table S1). **(A-B)** Analysis of the KF replication reactions with hTel-IM and ILPR-IM templates. The arrows indicate the intermediate bands in ILPR-IM. **(C-D)** Polymerization of two partial i-motif sequences at pH 6.2.

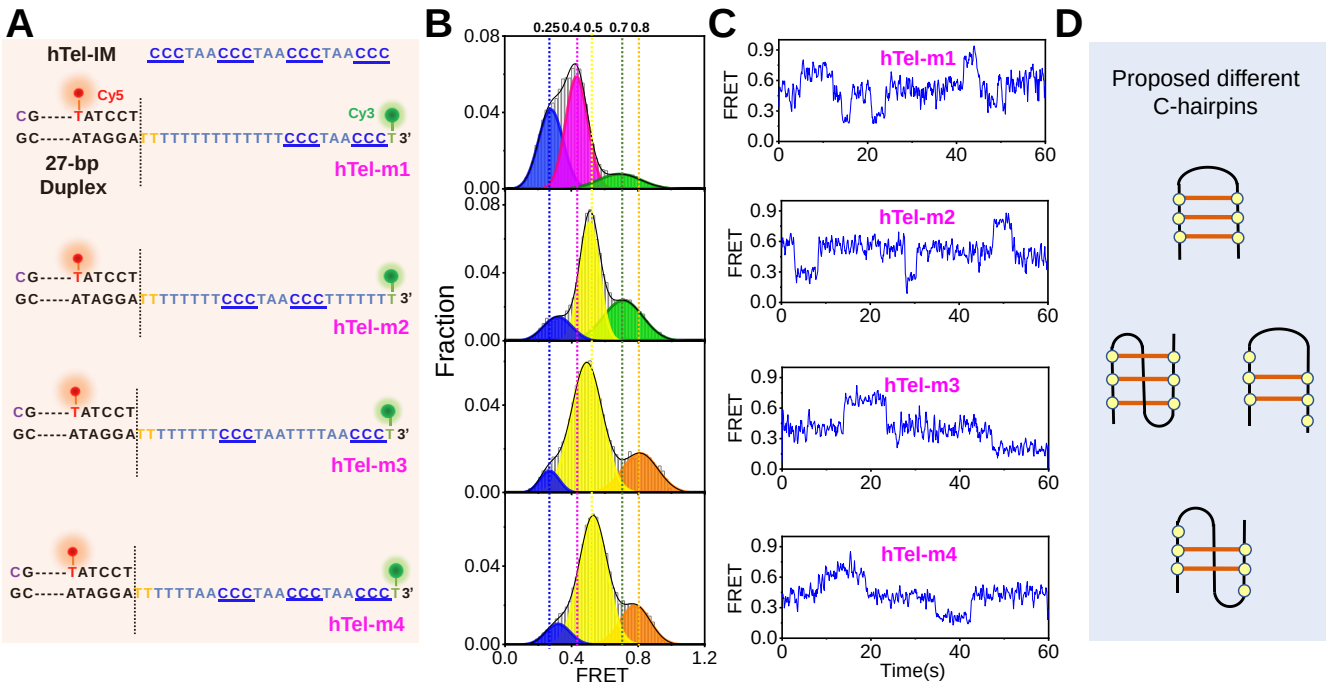

Figure S7. Different forms of C-hairpin are the probable folding intermediates of i-motif DNA. Related to Figure 2. (A) The schematic design of the ssDNA with partial i-motif sequences. Three or two C-tracts are included with different loop lengths. The acidic condition at pH 5.8 was used to promote the folding of higher-order structures. **(B)** FRET distributions of the structures formed by the partial i-motif sequences. **(C)** The representative FRET traces showing the dynamic changes of those structures. **(D)** The proposed C-hairpin structures formed by the partial i-motif sequences.

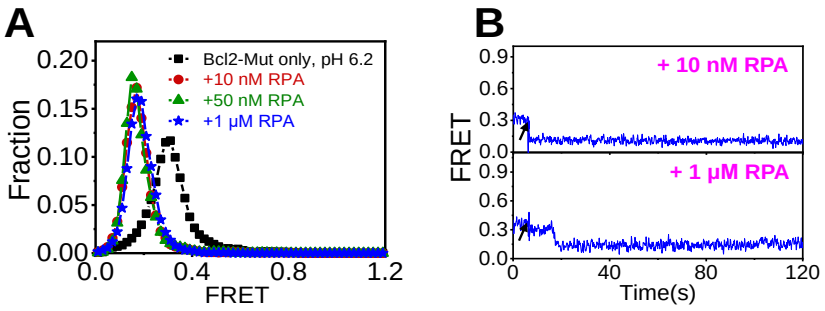

Figure S8. The Bcl2-Mut sequence can be bound and stretched by RPA at pH 6.2. Related to Figure 3. (A) FRET distributions of Bcl2-Mut at pH 6.2 before and 4 min after the addition of RPA. **(B)** The representative FRET traces with the addition of 10 nM to 1 μM RPA. The black arrows indicate the addition of protein.

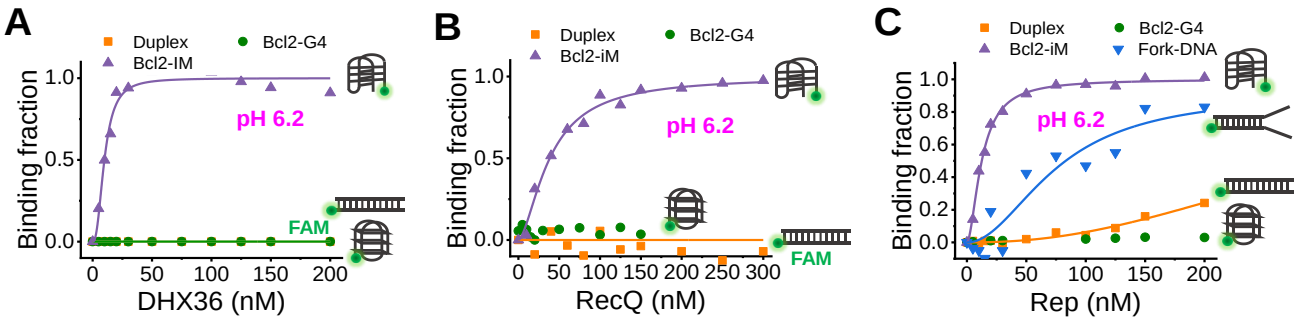

Figure S9. The binding of DHX36, RecQ, and Rep helicases with different DNA substrates at pH 6.2. Related to Figure 4. (A-C) Changes of DNA binding fractions with the increases in helicase concentrations. The binding curve was fitted by the Hill equation: $y = [protein]^n/(Kd^n+[protein]^n)$, where y is the binding fraction, n is the Hill coefficient, and *K*d is the apparent dissociation constant.

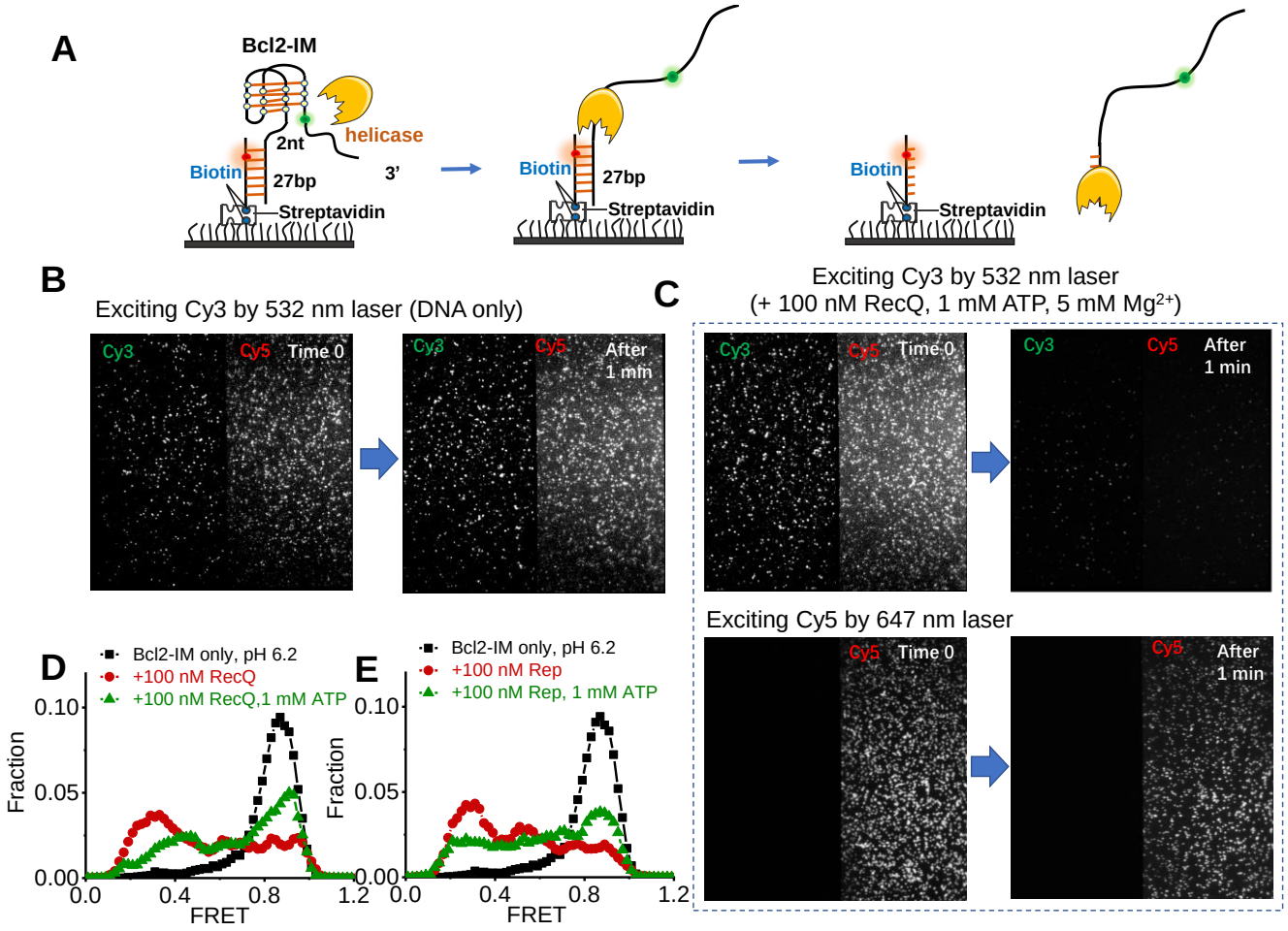

Figure S10. The effects of ATP on the activity of RecQ and Rep helicases. Related to Figure 5. (A) Once the downstream duplex was efficiently unwound by helicases at the ATP-hydrolysis state, the Cy3-strands would be released from the surface and the FRET distributions cannot be determined. Meanwhile, the Cy5-strands were still anchored at the surface. **(B)** Most of the fluorophores carried by the Bcl2-IM substrate did not undergo photobleaching within a time scale of 1 min excitation. **(C)** The upper panel shows that, upon the addition of helicases at the ATP hydrolysis state, taking RecQ for an example, both the Cy3 and Cy5 spots disappeared significantly with the excitation of Cy3 by the 532 nm laser. However, Cy5 fluorophores were still there when the 647 nm laser was turned on. The above two pieces of evidence together can reflect the unwinding of duplex DNA, as illustrated in Figure S10A. It is worth noting that the Cy5 spots we observed with the direct excitation by 647 nm laser were usually more than that with 532 nm laser, possibly because not every Cy5-strand has an annealed Cy3-strand or some Cy3 fluorophores in Cy3-strands were dead fluorophores. **(D-E)** FRET distributions of Bcl2-IM before and 4 min after the addition of RecQ and Rep at the apo, and ATP-binding states. The FRET distributions after the addition of RecQ and Rep at ATP hydrolysis state cannot be determined due to the significant disappearance of fluorescent spots.

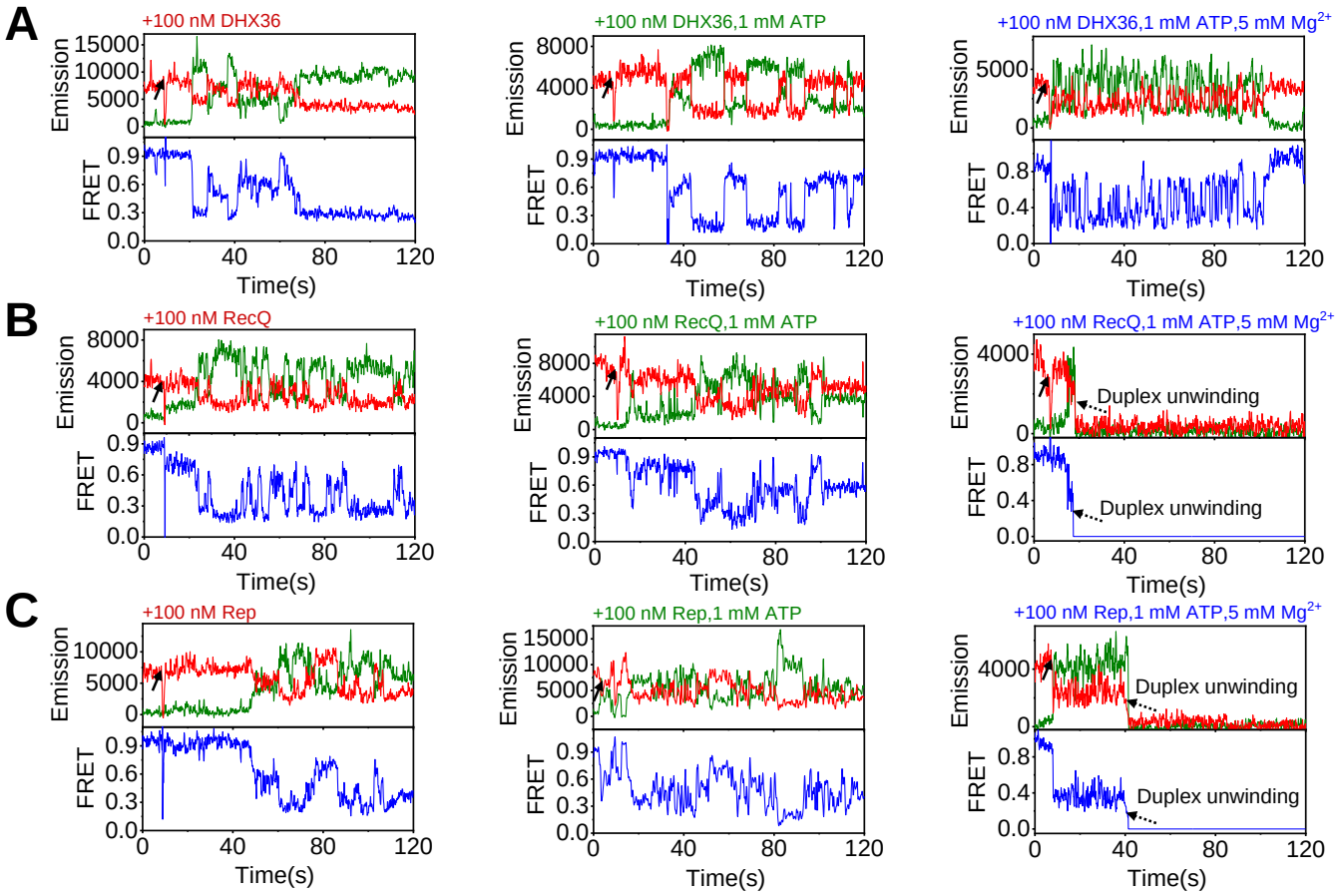

Figure S11. The representative fluorescence emission and FRET traces of Bcl2-IM with the addition of helicases. Related to Figure 5. (A) Traces of Bcl2-IM with the addition 100 nM DHX36 at the apo, ATP-binding, and ATP-hydrolysis states. **(B)** Traces of Bcl2-IM with the addition of 100 nM RecQ at the apo, ATP-binding, and ATP-hydrolysis states. With the hydrolysis of ATP, RecQ efficiently unwinds the duplex DNA downstream of the i-motif. **(C)** Typical traces of Bcl2-IM with the addition 100 nM Rep at the apo, ATP-binding, and ATP-hydrolysis states. The traces in the right panels of Figure S11B-C may most possibly reflect the unwinding of duplex DNA due to the simultaneous disappearance of Cy3 and Cy5 as illustrated in Figure S10 for the following reasons. First, the fluorescence of Cy3 is usually more stable than Cy5(1). In most cases of photobleaching, Cy5 would bleach earlier than Cy3; therefore, Cy3 may still last for a while after the disappearance of Cy5 signal, rather than drop at the same time. Second, the signal decreases occur at ~ 20-40 s in the above figures, obviously shorter than the life time of these fluorophores before photobleaching. However, it is worth noting that in some rare cases, due to the in advance photobleaching of Cy3, Cy5 and Cy3 may disappear simultaneously, displaying similar traces as above.

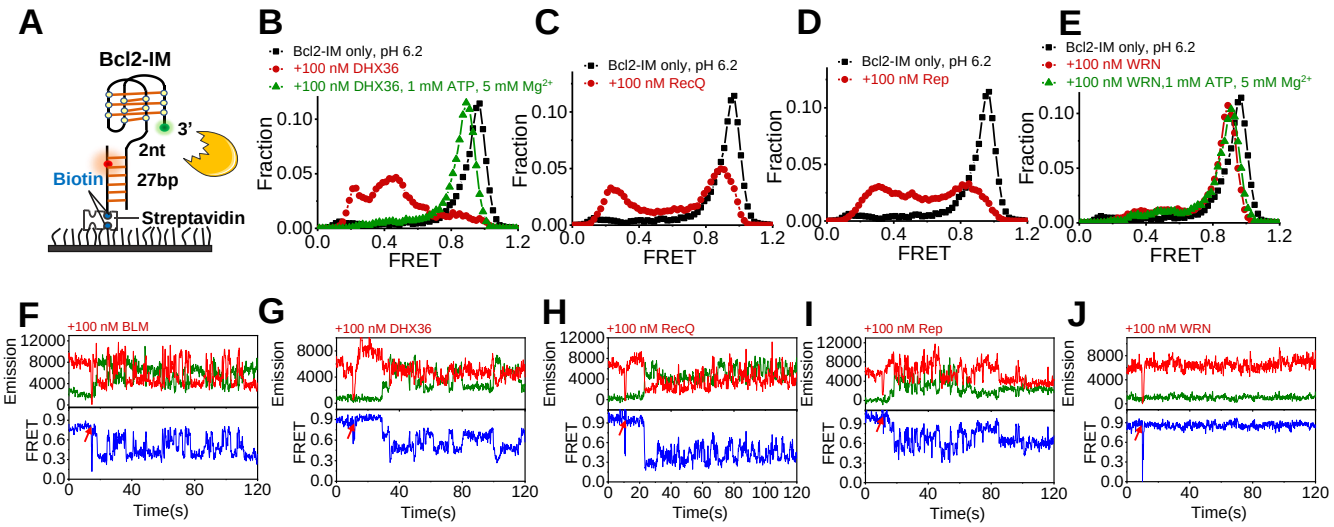

Figure S12. The ssDNA tail is dispensable for the helicases-mediated i-motif unfolding. Related to Figure 5. **(A)** The schematic design of Bcl2-IM substrate. **(B)** FRET distributions of Bcl2-IM before and 4 min after the addition of DHX36 at the apo and ATP-hydrolysis states. **(C-D)** FRET distributions of Bcl2-IM before and 4 min after the addition of RecQ and Rep. In the presence of ATP, the downstream duplex DNA was efficiently unwound; therefore, the FRET distributions cannot be determined. **(E)** FRET distributions of Bcl2-IM before and 4 min after the addition of WRN at the apo and ATP-hydrolysis states. **(F-J)** The representative traces with the addition of helicases.

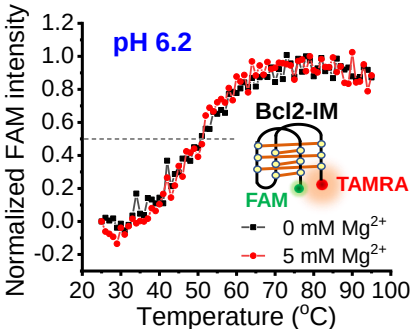

Figure S13. The effect of Mg^{2+} on the thermal stability of Bcl2-IM at pH 6.2. Related to Figure 5. No obvious changes in the T_m values can be observed with or without the addition of 5 mM Mg^{2+}.

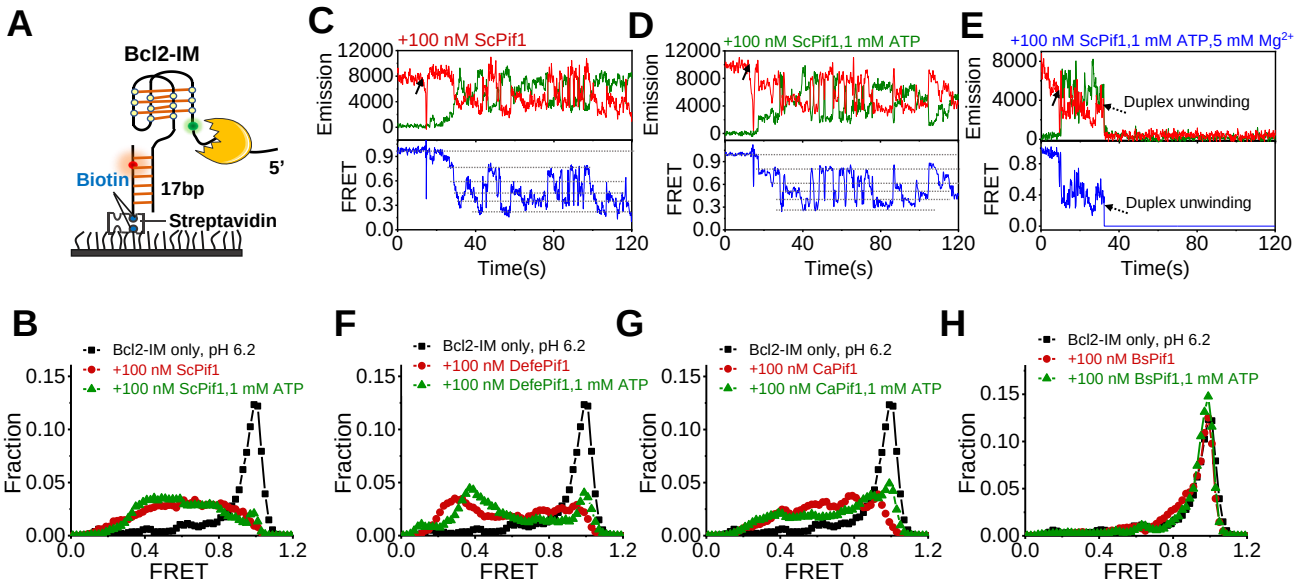

Figure S14. The 5'-3' helicases repetitively unfold Bcl2-IM in the ATP-independent mode. Related to Figure 5. (A) The schematic experimental design to characterize the unfolding of Bcl2-IM by the 5'-3' DNA helicases. **(B)** FRET distributions of Bcl2-IM before and 4 min after the addition of 100 nM Pif1 from *S. cerevisiae* at the apo and ATP-binding states. The downstream duplex was efficiently unwound once the helicase was at the ATP-hydrolysis state; therefore, the FRET distributions cannot be determined. **(C-E)** The representative fluorescence emission and FRET traces of Bcl2-IM with the addition of 100 nM Pif1 in different ATP states. **(F-H)** FRET distributions of Bcl2-IM before and 4 min after the addition of 100 nM Pif1 from other species.

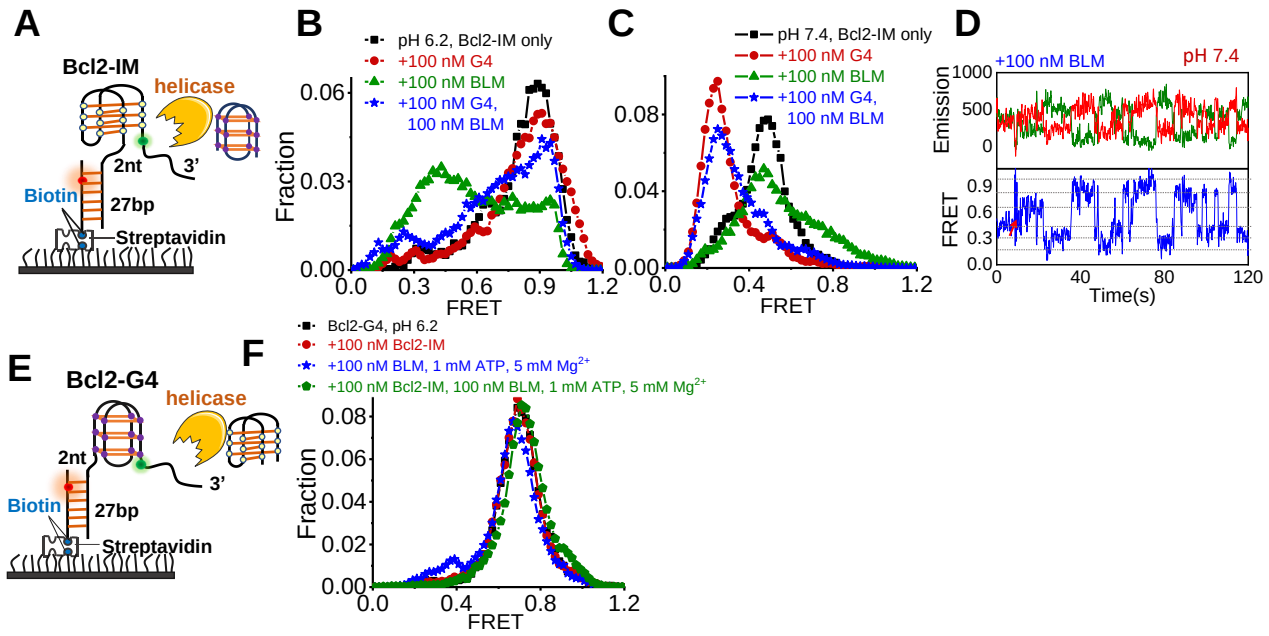

Figure S15. Competition FRET assay to define the BLM helicase behavior on Bcl2-IM and Bcl2-G4 in the presence of the complementary strands. Related to Figure 5 and Figure 6. (A) The experimental design to characterize the status of Bcl2-IM. In the first two experiments, 100 nM Bcl2-G4 or 100 nM BLM was added separately to Bcl2-IM as a control. In the third experiment, 100 nM Bcl2-G4 and 100 nM BLM helicases were mixed and then added simultaneously to the Bcl2-IM substrates. It is worth noting that, ATP hydrolysis significantly decreases the unfolding activity of BLM on Bcl2-IM as shown in Figure 5; therefore, ATP was not added here. **(B-C)** The FRET distributions of Bcl2-IM in different reaction conditions at pH 6.2 and pH 7.4. **(D)** The selective traces of Bcl2-IM at pH 7.4 with the addition of 100 nM BLM. **(E)** The experimental design to characterize the status of Bcl2-G4. In the first two experiments, 100 nM Bcl2-IM or 100 nM BLM was added seperately to Bcl2-G4 as a control. In the third experiment, 100 nM Bcl2-IM and 100 nM BLM helicases were mixed and then added simultaneously to the Bcl2-G4 substrates. It is worth noting that, ATP hydrolysis was essential for BLM to unfold Bcl2-G4 as shown in Figure 6; therefore, ATP was added here. **(F)** The FRET distributions of Bcl2-G4 in different reaction conditions at pH 6.2. BLM displays little disruptive effects on Bcl2-G4 at low pH regardless of the absence or presence of Bcl2-IM.

Table S1. DNA sequences used in this study. Related to STAR Methods

Names	Oligo sequences (5’-3’)
	sequences (5’-3’) of substrates for CD
Bcl2-IM	CCCGCCCCCTTCCTCCCGCGCCC
hTel-IM	CCCTAACCCTAACCCTAACCC
ILPR-IM	CCCCACACCCCTGTCCCCACACCCC
Bcl2-G4	GGGCGCGGGAGGAAGGGGGCGGG
hTel-G4	GGGTTAGGGTTAGGGTTAGGG
ILPR-G4	GGGGTGTGGGGACAGGGGTGTGGGG
Bcl2-Mut	CTCTCTCTCTTCCTCTCTCGCTC
random ssDNA	GTGTGGTGTTGGGCCCGCGC
	sequences (5’-3’) of substrates for FRET-melting assay
F-Bcl2-IM-T	**FAM** CCCGCCCCCTTCCTCCCGCGCCC **TAMRA**
F-hTel-IM-T	**FAM** CCCTAACCCTAACCCTAACCC**TAMRA**
F-ILPR-IM-T	**FAM** CCCCACACCCCTGTCCCCACACCCC **TAMRA**
F-Bcl2-G4-T	**FAM** GGGCGCGGGAGGAAGGGGGCGGG **TAMRA**
F-hTel-G4-T	**FAM** GGGTTAGGGTTAGGGTTAGGG **TAMRA**
F-ILPR-G4-T	**FAM** GGGGTGTGGGGACAGGGGTGTGGGG **TAMRA**
	sequences (5’-3’) of substrates for DNA polymerase stop assay
12-nt	**FAM** GATTTGATGTAC
18-nt	**FAM** GATTTGATGTACAAAAAA
41-nt	**FAM** GATTTGATGTACAAAAAAGGGCGCGGGAGGAAGGGGGCGGG
Bcl2-IMs12	**CCCGCCCCCTTCCTCCCGCGCCC**TTTTTTGTACATCAAATC
hTel-IMs12	**CCCTAACCCTAACCCTAACCC**TTTTTTGTACATCAAATC
ILPR-IMs12	**CCCCACACCCCTGTCCCCACACCCC**TTTTTTGTACATCAAATC
hTel-m2s12	**CCCTAACCCTAATTT**TTTTTTGTACATCAAATC
hTel-m4s12	**CCCTAACCCTAACCC**TTTTTTGTACATCAAATC
	sequences (5’-3’) of substrates for stopped-flow assay
16nt-F	CTCTGCTCGACGGATT **FAM**
H-d16s15	**HEX** AATCCGTCGAGCAGAGTTTTTTTTTTTTTTT
	sequences (5’-3’) of substrates for binding assay
24nt-F	GCCCTGGTGCCGACCAACGAAGGT **FAM**
24nt	ACCTTCGTTGGTCGGCACCAGGGC
d2012nt-F	CACTGGCCGTCTTACGGTCGCTCTGCTCGACG **FAM**
d2012nt	CGTCGAGCAGAGCGACCGTATTATTTTTTTTT
F-Bcl2-G4	**FAM** GGGCGCGGGAGGAAGGGGGCGGG
F-Bcl2-IM	**FAM** CCCGCCCCCTTCCTCCCGCGCCC

Names	Oligo sequences (5’-3’)
	sequences (5’-3’) of substrates for smFRET
d27Bcl2-IM	GCGTGGCACCGGTAATAGGAAATAGGATT**CCCGCCCCCTTCCTCCCGCGCCC**T-Cy3
d27hTel-IM	GCGTGGCACCGGTAATAGGAAATAGGATT**CCCTAACCCTAACCCTAACCC**T-Cy3
d27ILPR-IM	GCGTGGCACCGGTAATAGGAAATAGGATT**CCCCACACCCCTGTCCCCACACCCC**T-Cy3
d27Bcl2-Mut	GCGTGGCACCGGTAATAGGAAATAGGATT**CTCTCTCTCTTCCTCTCTCGCTC**-Cy3
d27hTel-m1	GCGTGGCACCGGTAATAGGAAATAGGATT**TTTTTTTTTTTTCCCTAACCC**T-Cy3
d27hTel-m2	GCGTGGCACCGGTAATAGGAAATAGGATT**TTTTTTCCCTAACCCTTTTTT**T-Cy3
d27hTel-m3	GCGTGGCACCGGTAATAGGAAATAGGATT**TTTTTTCCCTAATTTTAACCC**T-Cy3
d27hTel-m4	GCGTGGCACCGGTAATAGGAAATAGGATT**TTTTTTCCCTAACCCTAACCC**T-Cy3
d27Bcl2-IMs14	GCGTGGCACCGGTAATAGGAAATAGGATT**CCCGCCCCCTTCCTCCCGCGCCC**T(iCy3)TTTTTTTTTTTTT
d27Bcl2-G4s14	GCGTGGCACCGGTAATAGGAAATAGGATT**GGGCGCGGGAGGAAGGGGGCGGG**T(iCy3)TTTTTTTTTTTTT
Stem	TCCTAT(iCy5)TTCCTATTACCGGTGCCACGC-Biotin
Bcl2-G4d15	Cy5-G**GGCGCGGGAGGAAGGGGGCGGG**TTGTATGACAAGGAAGG
s14Bcl2-IMd15	TTTTTTTTTTTTT**T(iCy3)TCCCGCCCCCTTCCTCCCGCGCCC**TTGTATGACAAGGAAGG
Stem	Biotin-CCTTCCTTGTCAT(iCy5)AC

All the internal fluorophores were labeled via the base thymine.

Table S2. The *K*d values resulted from fitting. Related to Figure 4 and Figure S9.

	BLM		DHX36		RecQ		Rep	
	*K*d	*Error*	*K*d	*Error*	*K*d	*Error*	*K*d	*Error*
Duplex	*	*	*	*	*	*	329.9	±51
Fork	101.4	±17.0	*	*	*	*	76.04	±32
Bcl2-G4	97.7	±28.1	*	*	*	*	*	*
Bcl2-IM	22.0	±3.7	9.9	±0.7	38.5	±3.5	12.5	±0.5

* denotes the binding curves were not available or could not be fitted due to the poor binding affinity.

Table S3. The number of FRET traces used in the FRET distributions. Related to Figures 1-7.

		pH 6.2	pH 6.6	pH 7.0	pH 7.4	pH 8.0
Figure 2B	Bcl2-iM	350	376	412	475	394
Figure S4B	Bcl2-G4	319	306	378	263	304
Figure S1D	Bcl2-Mut	375	401	327	360	350
Figure 5B	hTel-iM	442	514	346	308	479
Figure 5G	ILPR-iM	453	438	483	325	368
		pH 5.8				
Figure S7B	hTel-m1	299				
	hTel-m2	459				
	hTel-m3	312				
	hTel-m4	338				
		+10 nM	+50 nM RPA	+1μM		
Figure 3B	Bcl2-iM	277	292	258		
Figure S8A	Bcl2-Mut	329	472	303		
		+BLM	+BLM+ATP	+BLM+ATP+Mg^{2+}		
Figure 5H	Bcl2-iM	341	*	408		
Figure 5B	Bcl2-iMT14,	367	409	317		
Figure 6B	Bcl2-G4T14, pH 6.2	328	*	354		
Figure 6C	Bcl2-G4T14, pH 7.4	357	*	398		
		+DHX36	+DHX36+ATP	+DHX36+ATP+Mg^{2+}		
Figure S12B	Bcl2-iM	344	*	449		
Figure 5F	Bcl2-iMT14	501	423	279		
Figure 6E	Bcl2-G4T14	406	*	409		
		+RecQ	+RecQ+ATP	+RecQ+ATP+Mg^{2+}		
Figure S12C	Bcl2-iM	386	*	*		
Figure S10D	Bcl2-iMT14	495	346	*		
Figure 6F	Bcl2-G4T14	365	*	346		
		+Rep	+Rep+ATP	+Rep+ATP+Mg^{2+}		
Figure S12D	Bcl2-iM	301	*	*		
Figure S10E	Bcl2-iMT14	329	279	*		
Figure 6G	Bcl2-G4T14	419	*	348		
		+WRN	+WRN+ATP+Mg^{2+}			
Figure S12E	Bcl2-iM	331	447			
		+ScPif1	+ScPif1+ATP			
Figure S14B	T14Bcl2-iM	360	285			
		+DefePif1	+DefePif1+ATP			
Figure S14F	T14Bcl2-iM	450	296			
		+CaPif1	+CaPif1+ATP			
Figure S14G	T14Bcl2-iM	348	297			
		+BsPif1	+BsPif1+ATP			
Figure S14H	T14Bcl2-iM	363	265			
		+G4	+BLM	+G4+BLM		
Figure S15B	Bcl2-iMT14, pH 6.2	462	367	324		
Figure S15C	Bcl2-iMT14, pH 7.4	331	301	363		
Figure S15F	Bcl2G4T14+iM	402				
	Bcl2-G4T14+iM+BLM+ATP+Mg^{2+}	338				

* denotes that the substrates were efficiently unwound by helicases or under this condition no experiment has been carried out